Journal of Materials Chemistry C

Accepted Manuscript

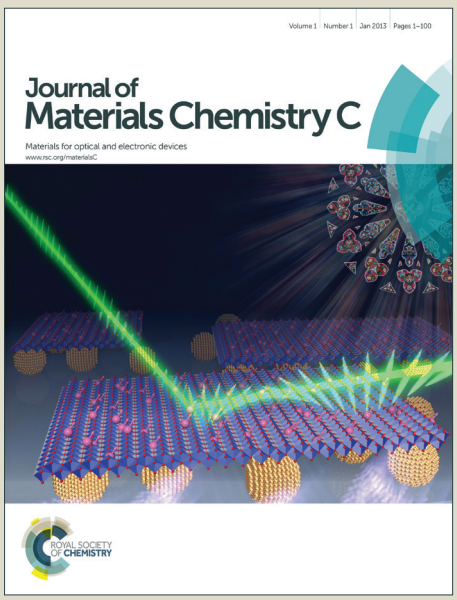

ROYAL SOCIETY OF CHEMISTRY

www.rsc.org/materialsC

Nd Doping Bismuth Ferrite to Tune Electromagnetic Properties and Increase Microwave Absorption by Magnetic-dielectric Synergy

Yong Li,[a] Wen-qiang Cao,[b] Jie Yuan,*[b] Da-wei Wang[a] and Mao-sheng Cao*[a]

[a]School of Material Science and Engineering, Beijing Institute of Technology, Beijing, 10008, China

E-mail: caomaosheng@bit.edu.cn

[b]School of Science, Minzu University of China, Beijing 10008, China

E-mail: yuanjie4000@sina.com

Simultaneously achieving tunable electromagnetic parameters and strong absorption capacity in a single material is still a great challenge. Here, we present Nd doped $BiFeO_3$ with electromagnetic matching, which exhibits tunable electromagnetic properties and high-performance microwave absorption. The experimental and calculated results demonstrate that Nd doping generates the ordering domains structure and changes the electrons coupling states, which induce difficult polarization rotation and strong natural ferromagnetic resonance, leading to the decrease of dielectric loss and the increase of magnetic loss with increasing Nd concentration. The electromagnetic parameters are tuned from mismatching to matching, and the microwave absorption is improved. $Bi_{0.8}Nd_{0.2}FeO_3$ exhibits remarkable reflection loss (*RL*) of -42 dB and bandwidth ($RL \leq$ -10 dB) which covers nearly three quarters of X-band at the thickness from 1.9 to 2.1 mm. This work highlights the applications of BFO as a high-performance microwave absorber and opens up a promising feasible route to the development of microwave absorbers in imaging, healthcare, information safety and military fields.

High-performance microwave absorbers with high efficiency and broadband absorption are intensively pursued owing to their potential applications in healthcare, signal and data protection and national defense security.[1-4] Recently, various novel microwave absorbers have been developed. Carbon nanomaterials, such as carbon nanotubes and graphene, have grabbed much attention for electromagnetic (EM) wave attenuation due to low density, high aspect ratio and high

conductivity.[1,5-9] Unfortunately, only relying on dielectric and conduction loss, the absorption capacity of carbon nanomaterials is low. Magnetic materials are another attractive candidate for microwave absorption, of which physical or chemical properties can be readily controlled through size, shape and dimension.[10-14] A drawback, however, is narrow absorption bandwidth. Dielectric-magnetic hybrid materials with good absorption capacity are praised highly,[15-18] which results from efficient complementarities between the permittivity and permeability in materials.[19] Nonetheless, their applications are limited by the complex fabrication and relatively low output capacity. Tuning EM parameters and improving absorption capacity, therefore, is still a highly challenge, which becomes more difficult in view of simple and economy fabrication. It is quite necessary to search for a new microwave absorber consisting of a single material, which needs to possess prominent dielectric and magnetic properties simultaneously and achieve magnetic-dielectric synergy with EM matching.

As a fascinating multifunction material, $BiFeO_3$ (BFO) exhibits outstanding ferroelectric and antiferromagnetic properties, and many unexpected advantages such as coupling to spintronics, conduction at domain walls.[20-22] Furthermore, it possesses both dielectric loss and magnetic loss, which has opened new perspectives for BFO as a microwave absorber. BFO nanoparticles, ceramics and composites show good microwave absorption.[23-26] Doped BFO materials increase microwave absorption based on enhancement of magnetism.[26,27] The absorption performance is shown in Tab. S1. The absorption capacity, bandwidth and thickness, however, still need to be improved further owing to EM mismatching, and the relationship between structure and microwave absorption is rarely explored. Here we demonstrate the tunable EM properties and high-performance microwave absorption of $Bi_{1-x}Nd_xFeO_3$ (BNFO). With the increase of Nd concentration, the reflection loss (*RL*) and bandwidth of BNFO increase in the frequency range of 8.2–12.4 GHz (X-band). When Nd concentration is 0.20, the *RL* reaches -42 dB and bandwidth ($RL \leq$ -10 dB) covers nearly three quarters of X-band at the thickness of 1.9, 2.0 and 2.1 mm. The high-performance microwave absorption of BNFO is more excellent than that in the literature (Tab. S1), which is attributed to the

formation of ordering domain structure and the strengthening of superexchange interaction through Nd doping, which play important roles in tuning dielectric loss and magnetic loss to reach a balance, resulting in achieving EM matching in a single material.

Fig.1a-c shows the transmission electron microscopy (TEM) images of BFO and BNFO powders. The particles size is about 20–90 nm. The scanning electron microscope (SEM) images show that the particles have the random shapes (Fig. S1). The X-ray diffraction (XRD) patterns show that BFO is single phase perovskite with the *R*3*c* space group, while BNFO20 (x = 0.20) possesses the $PbZrO_3$-like structure with the *Pbam* space group (Fig. S2a and S2b), which has also been reported in the previous literature.[28] In the intermediate compositions, BNFO5, BNFO10 and BNFO15 (x = 0.05, 0.10 and 0.15), the *R*3*c* phase and the *Pbam* phase coexist, and the *Pbam* phase increases with the increase of Nd concentration (Fig. S2c). The Raman spectroscopy results illustrate that the structural evolution is attributed to the substitution of Nd for Bi, which weakens the hybridization of Bi 6*s* and O 2*p* orbits, leading to the decrease of the distortion of BFO (Fig. S3).[20]

The high-resolution TEM (HRTEM) images are shown in Fig. 1d-f. For BFO, the interplanar spacing is about 0.27 and 0.28 nm, corresponding to the (110) and (104) crystal plane of BFO with *R*3*c* phase, respectively. For BNFO10, ordering domain structure (O_d) appears, and the O_d regions and disordering structure (D) regions coexist. With the increase of Nd concentration, the O_d regions are expanded (Fig. 1f). The wavelength of ordered superlattice modulation is 0.79 nm, which corresponds to the double of the (120) interplanar spacing (the inset in Fig. 1f). The O_d structure is not observed in BFO, due to structural disorder of BFO.[29,30] The selected area electron diffraction (SAED) patterns of BFO and BNFO20 are shown in Fig. 1g and 1h, respectively. Compared with BFO, BNFO20 exhibits the $^1/_2$(120) type superlattice reflection, indicating the presence of ordering structure. Fig. 1i shows the one-dimensional diffraction profiles of the SAED patterns for BFO and BNFO20 using a XRD analysis package.[31] The results coincide with the XRD patterns of the powders.

The three-dimensional (3D) plots of the real permittivity (ε') and imaginary permittivity (ε'') of BFO and BNFO in the frequency range 8.2–12.4 GHz are shown in Fig. 2a and 2b, respectively. Both the ε' and the ε'' decrease with increasing frequency. With the increase of Nd concentration, the ε' increases while the ε'' decreases. The ε'' decreases by 30% from BFO to BNFO20 (Fig. 2c). According to Debye equation, the conduction part (ε_c'') and the polarization part (ε_p'') of imaginary permittivity are obtained (Fig. S4). The ε_c'' is in the magnitude of 10^{-6}–10^{-4} which is much smaller than the ε_p'' **(**Fig. 2d). Therefore, the main contribution to permittivity of BFO and BNFO is polarization rather than conduction. The Cole-Cole plots show two semicircles for BFO and BNFO, indicating that two polarizations exist in the BFO system (Fig. S5). X-ray photoelectron spectroscopy (XPS) results reveal that oxygen vacancies exist in BFO and BNFO (Fig. S6). The polarization may be induced by intrinsic dipole and defect dipole, which are caused by the lone pair of Bi ion and oxygen vacancy. In addition, interfacial polarization between the particles may be formed in BFO and BNFO. Compared with the dipole polarizations, the interface polarization is weak due to the similar polarity and conductivity between the particles, which does not cause the corresponding Cole-Cole semicircle. Hence, the main contribution to permittivity is the dipole polarizations. Based on the characteristics of microstructure, the disordering structure of BFO leads to disorder in the dipoles, thus the polarization has different orientation as shown in Fig. 2e. For the intermediate compositions, the polarization in the *D* regions shows the similar situation to that of BFO, while the O_d regions exhibit uniform orientation of polarization owing to ordered dipoles. The ordered dipoles interaction in an O_d region can induce a giant dipole,[32] which plays an important role in enhancing polarization. With the expanding of the O_d regions, the polarization increases, leading to the increase of the ε'. Moreover, the bulky giant dipoles are difficult to rotate at such high frequency. This causes less energy loss, reflecting in the decrease of the ε''.

The real permeability (μ') and imaginary permeability (μ'') of BFO and BNFO are shown in Fig. 3a and 3b. Both the μ' and the μ'' increase with the increase of Nd concentration. The average μ'' of BNFO20 is almost 550% higher than that of BFO. The increase of the μ' is attributed to increase of

magnetization, which is proved by the increase of the saturation magnetizations and remnant magnetizations (Fig. S7). The increase of the magnetization is associated with the structure and electron structure of BNFO. The O_d can suppress cycloidal spin of BFO to increase magnetization. In addition, the strengthening of the superexchange interaction by hybridizing between Fe 3*d* and O 2*p* orbitals increases magnetization as well. The densities of states of Fe 3*d*, 4*s* and O 2*p* electrons of BFO and BNFO show that the spin splitting (Δ) of the spin up and spin down for BNFO is bigger than that for BFO, implying that BNFO possesses stronger superexchange interaction (Fig. 3c and 3d). The complete densities of states are shown in Fig. S8. It is known that the occupancy of the 3*d* states is the critical factor in determining the strength of exchange interaction. The electrons coupling states of the superexchange interaction in BFO and BNFO are shown in Fig. 3e and 3f, respectively. Nd doping weakens the hybridization of O 2*p* and Bi 6*s* orbits and shortens the average distance of Fe and O from 2.0220 Å to 2.0105 Å, resulting in that the O 2*p* electrons in BNFO have higher probability to occupy Fe 3*d* orbitals than that in BFO. Thus the superexchange interaction is strengthened, leading to the increase of the μ'.

The eddy current coefficients $\mu''(\mu')^{-2}f^{-1}$ of BFO and BNFO change with increasing frequency, indicating that the magnetic loss is not caused by eddy current loss (Fig. S9).[19] It is suggested that magnetic loss of nano-sized BFO and BNFO in GHz frequency range originates from natural ferromagnetic resonance,[33] i.e. the equal and opposite magnetization vectors (*M*) precess around the direction of the effective field (H_{eff}) (Fig. 3e and 3f). The H_{eff} consists of anisotropy field and exchange interaction field. The coercive field increases with the increase of Nd concentration (Fig. S7), indicating the enhancement of the anisotropy field intensity due to the O_d.[34] The stronger superexchange interaction enhance the exchange interaction field intensity. Hence, the increase of the H_{eff} strengthens natural ferromagnetic resonance, resulting in the increase of the μ''.

Nd doping tunes the permittivity and permeability by controlling structure and modulating electron structure which provide potential application for BNFO in microwave absorption. Fig. 4a-e shows the 3D plots of *RL* versus frequency and thickness (*d*) for BFO and BNFO. It is observed that

the absorption region with the $RL \leq$ -10 dB is broadened and shifts towards lower thickness with the increase of Nd concentration. The widest absorption bandwidth ($RL \leq$ -10 dB) is obtained in BNFO20, which is nearly 3 GHz, about 130 % of that of BFO. Furthermore, BNFO has an absorption region with the $RL \leq$ -20 dB, which is broadened with the increase of Nd concentration. BNFO20 has three absorption regions with the $RL \leq$ -30 dB in the investigated ranges of frequency and thickness. The minimum (Min.) *RL* is -17 dB for BFO with d = 2.4 mm. The Min. *RL* of BNFO20 reaches -42 dB (d = 2.3 mm), which exceeds the *RL* of BFO materials in the literatures (Tab. 1S). Fig. 4f shows that the Min. *RL* increases with the increase of Nd concentration. These results indicate that Nd doping into BFO can effectively increase microwave absorption, broaden bandwidth and decrease effective absorption thickness.

Fig. 5a shows the *RL* of BFO and BNFO at d = 2.3 mm. With the increase of Nd concentration, the absorption peak shifts to low frequency, and the intensity of the absorption peak increases, where the Min. *RL* of BNFO20 is almost 2.5 times higher than that of BFO. At other thicknesses, the *RL* of BFO and BNFO shows similar change trend (Fig. S10). For BNFO20, the absorption peak shifts to low frequency with increasing thickness, and the Min. *RL* surpasses -20 dB at the investigated thicknesses (Fig. 5b). The increase of microwave absorption for BNFO is attributed to EM matching in the frequency and thickness ranges investigated. The dielectric loss ($\tan\delta_e$) and the magnetic loss ($\tan\delta_m$) versus Nd concentration are shown in the inset of Fig. 5a. For BFO, the $\tan\delta_e$ and the $\tan\delta_m$ are out of balance, reflecting EM mismatching, which leads to poor microwave absorption. With the increase of Nd concentration, the $\tan\delta_e$ decreases moderately and the $\tan\delta_m$ increases caused by difficult polarization rotation and strong natural ferromagnetic resonance respectively, due to the formation of the O_d and the strengthening of superexchange interaction. The decrease of the $\tan\delta_e$ and the increase of the $\tan\delta_m$ achieve the development of EM parameters from mismatching to matching. Compared with BFO, BNFO20 shows a relatively balance between the $\tan\delta_e$ and the $\tan\delta_m$ in the entire X-band (the inset of Fig. 5b), indicating EM matching,[35] thus it has the high-performance microwave absorption.

In conclusion, Nd doped BFO demonstrates tunable EM properties and high-performance microwave absorption. BNFO generates the O_d and changes the electrons coupling states, which induce the formation of the giant dipole and strengthen the superexchange interaction, leading to difficult polarization rotation and strong natural ferromagnetic resonance. Thus the $\tan\delta_e$ and the $\tan\delta_m$ tend to balance gradually with the increase of Nd concentration. BNFO20 exhibits EM matching, which has excellent *RL* of -42 dB and lower effective absorption thickness. The absorption bandwidth ($RL \leq$ -10 dB) of BNFO20 is broadened and covers three quarters of X-band, and three absorption regions with $RL \leq$ -30 dB appear in the investigated ranges of frequency and thickness. Nd doping expands the applications of BFO as a new family of microwave absorbers and provides a feasible strategy for the development of absorbers in communications, imaging, signal and data protection, and health detection fields.

Acknowledgements

This research was supported by the National Science Foundation of China (Grant Nos.51372282, 51402005 and 51132002).

Notes and References

1 Y. Zhang, Y. Huang, T. F. Zhang, H. C. Chang, P. S. Xiao, H. H. Chen, Z. Y. Huang and Y. S. Chen, *Adv. Mater.* 2015, **27**, 2049.
2 T. Xia, C. Zhang, N. A. Oyler and X. B. Chen, *Adv. Mater.* 2013, **25**, 6905.
3 H. J. Yang, M. S. Cao, Y. Li, H. L. Shi, Z. L. Hou, X. Y. Fang, H. B. Jin, W. Z. Wang and J. Yuan, *Adv. Optical Mater.* 2014, **2**, 214.
4 W. Li, U Guler, N Kinsey, G. V. Naik, A Boltasseva, J. G. Guan, V. M. Shalaev and A. V. Kildishev, Adv. Mater. 2014, **26**, 7959.
5 H. Sun, R. C. Che, X. You, Y. S. Jiang, Z. B. Yang, J. Deng, L. B. Qiu and H. S. Peng, *Adv. Mater.* 2014, **26**, 8120.
6 B. Wen, M. S. Cao, M. M. Lu, W. Q. Cao, H. L. Shi, J. Liu, X. X. Wang, H. B. Jin, X. Y. Fang, W. Z. Wang and J. Yuan, *Adv. Mater.* 2014, **26**, 3484.
7 Z. P. Chen, C. Xu, C. Q. Ma, W. C. Ren and H. M. Cheng, *Adv. Mater.* 2013, **25**, 1296.
8 M. K. Han, X. W. Yin, L. Kong, M. Li, W. Y. Duan, L. T. Zhang and L. F. Cheng, *J. Mater. Chem. A* 2014, **2**, 16403.
9 W. W. Liu, H. Li, Q. P. Zeng, H. N. Duan, Y. P. Guo, X. F. Liu, C. Y. Sun and H. Z. Liu, *J. Mater. Chem. A* 2015, **3**, 3739.
10 G. B. Sun, B. X. Dong, M. H. Cao, B. Q. Wei and C. W. Hu, *Chem. Mater.* 2011, **23**, 1587.
11 G. X. Tong, F. F. Du, L. J. Xiang, F. T. Liu, L. L. Mao and J. G. Guan, *Nanoscale* 2014, **6**, 778.
12 M. Zhou, X. Zhang, J. M. Wei, S. L. Zhao, L. Wang and B. X. Feng, *J. Phys. Chem. C* 2011, **115**, 1398.

13 Y. P. Duan, Z. Liu, H. Jing,Y. H. Zhang and S. Q. Li, *J. Mater. Chem.* 2012, **22**, 18291.
14 X. A. Fan, J. G. Guan, Z. Z. Li, F. Z. Mou, G. X. Tong and W. Wang, *J. Mater. Chem.* 2010, **20**, 1676.
15 H. Wang, L. N. Wu, J. F. Jiao, J. G. Zhou, Y. J. Xu, H. Y. Zhang, Z. H. Jiang, B. Z. Shen and Z. J. Wang, *J. Mater. Chem. A* 2015, **3**, 6517.
16 J. W. Liu, R. C. Che, H. J. Chen, F. Zhang, F. Xia, Q. S. Wu and M, Wang, *Small*, 2012, **8**, 1214.
17 G. Z. Wang, X. G. Peng, L. Yu, G. P. Wan, S. W. Lin and Y. Qin, *J. Mater. Chem. A* 2015, **3**, 2734.
18 C. Y. Liang, C. Y. Liu, H. Wang, L. N. Wu, Z. H. Jiang, Y. J. Xu, B. Z. Shen and Z. J. Wang, *J. Mater. Chem. A* 2014, **2**, 16397.
19 G. Z. Wang, Z. Gao, S. W. Tang, C. Q. Chen, F. F. Duan, S. C. Zhao, S. W. Lin, Y. H. Feng, L. Zhou and Y. Qin, *ACS Nano* 2012, **6**, 11009.
20 G. Catalan and J. F. Scott, *Adv. Mater.* 2009, **21**, 2463.
21 P. Rovillain, R. de Sousa, Y. Gallais, A. Sacuto, M. A. Méasson, D. Colson, A. Forget, M. Bibes, A. Barthélémy and M. Cazayous Nat. Mater. 2010, **9**, 975.
22 J. Seidel, L. W. Martin, Q. He, Q. Zhan, Y. H. Chu, A. Rother, M. E. Hawkridge, P. Maksymovych, P. Yu, M. Gajek, N.Bajke, S. V. Kalinin, S. Gemming, F. Wang, G. Catalan, J. F. Scott, N. A. Spaldin, J. Orenstein and R. Ramesh, Nat. Mater. 2009, **8**, 229.
23 Y. Q. Kang, M. S. Cao, J. Yuan and X. L. Shi, *Mater. Lett.* 2009, **63**, 1344.
24 F. S. Wen, N. Wang and F. Zhang, *Solid State Commun.* 2010, **150**, 1888.
25 J. Yuan, Z. L. Hou, H. J. Yang, Y. Li, Y. Q. Kang, W. L. Song, H. B. Jin, X. Y. Fang and M. S. Cao, *Ceram. Int.* 2013, **39**, 7241.
26 Z. L. Hou, H. F. Zhou, L. B. Kong, H. B. Jin, X. Qi and M. S. Cao, *Mater. Lett.* 2012, **84**, 110.
27 Y. Li, H. J. Yang, W. G. Yang, Z. L. Hou, J. B. Li, H. B. Jin, J. Yuan and M. S. Cao, *Mater. Lett.* 2013, **111**, 130.
28 S. Karimi, I. M. Reaney, I. Levin and I. Sterianou, *Appl. Phys. Lett.* 2009, **94**, 112903-1.
29 V. Petkov, S. M. Selbach, M. A. Einarsrud, T. Grande and S. D. Shastri, *Phys. Rev. Lett.* 2010, **105**, 185501-1.
30 C. L. Jia, L. Jin, D. W. Wang, S. B. Mi, M. Alexe, D. Hesse, H. Reichlova, X. Marti, L. Bellaiche and K. W. Urban, *Acta Mater.* 2015, **82**, 356.
31 H. Shi, G. Zhang, B. Zou, M. Luo and W. Wang, *Microsc. Res. Techniq.* 2013, **76**, 641.
32 D. V. Talapin and E. V. Shevchenko, *Nano Lett.* 2007, **7**, 1213.
33 L. B. Kong, Z.W. Li, L. Liu, R. Huang, M. Abshinova, Z. H. Yang, C. B. Tang, P. K. Tan, C. R. Deng and S. Matitsine, *Int. Mater. Rev.* 2013, **58**, 203.
34 N. Wang, L. Guo, L. He, X. Cao, C. P. Chen, R. M. Wang and S. H. Yang, *Small* 2007, **3**, 606.
35 M. S. Cao, R. R. Qin, C. J. Qiu and J. Zhu, *Mater. Des.* 2003, **24**, 391.

Figure captions

Fig. 1 TEM images of (a) BFO, (b) BNFO10 and (c) BNFO20 powders. HRTEM images of (d) BFO, (e) BNFO10 and (f) BNFO20, the inset in Fig. 1f is the schematic of the crystal structure corresponding to the O_d regions. The SAED patterns of (g) BFO and (h) BNFO20, the superlattice reflection is highlighted by blue circle. (i) The one-dimensional diffraction profiles of the BFO and BNFO20 generated by the SAED patterns.

Fig. 2 The 3D plots of (a) real permittivity and (b) imaginary permittivity versus frequency and Nd concentration, the arrows represent the increasing direction of permittivity. (c) The imaginary permittivity versus Nd concentration at various frequencies. (d) The polarization part and conduction part of imaginary permittivity versus Nd concentration at various frequencies. (e) Schematic illustrations of the polarization in BFO, intermediate compositions and BNFO20.

Fig. 3 The 3D plots of (a) real permeability and (b) imaginary permeability versus frequency and Nd concentration, the arrows represent the increasing direction of permeability. The densities of states for Fe 3*d*, 4*s* and O 2*p* electrons of (c) BFO and (d) BNFO. Schematic illustrations of the electrons coupling states of the superexchange interaction in (e) BFO and (f) BNFO.

Fig. 4 The 3D plots of *RL* versus frequency and thickness for (a) BFO, (b) BNFO5, (c) BNFO10, (d) BNFO15 and (e) BNFO20. (f) The Min. *RL* at different thickness versus Nd concentration. The *RL* values were calculated by the measured complex permittivity and permeability values according to the transmission line theory.

Fig. 5 (a) The *RL* of BFO and BNFO at the thickness of 2.3 mm, the inset shows the changes of the $\tan\delta_e$ and the $\tan\delta_m$ at various frequencies with increasing Nd concentration. (b) The *RL* of BNFO20 at various thicknesses, the inset shows the $\tan\delta_e$ and the $\tan\delta_m$ of BFO and BNFO20 versus frequency.

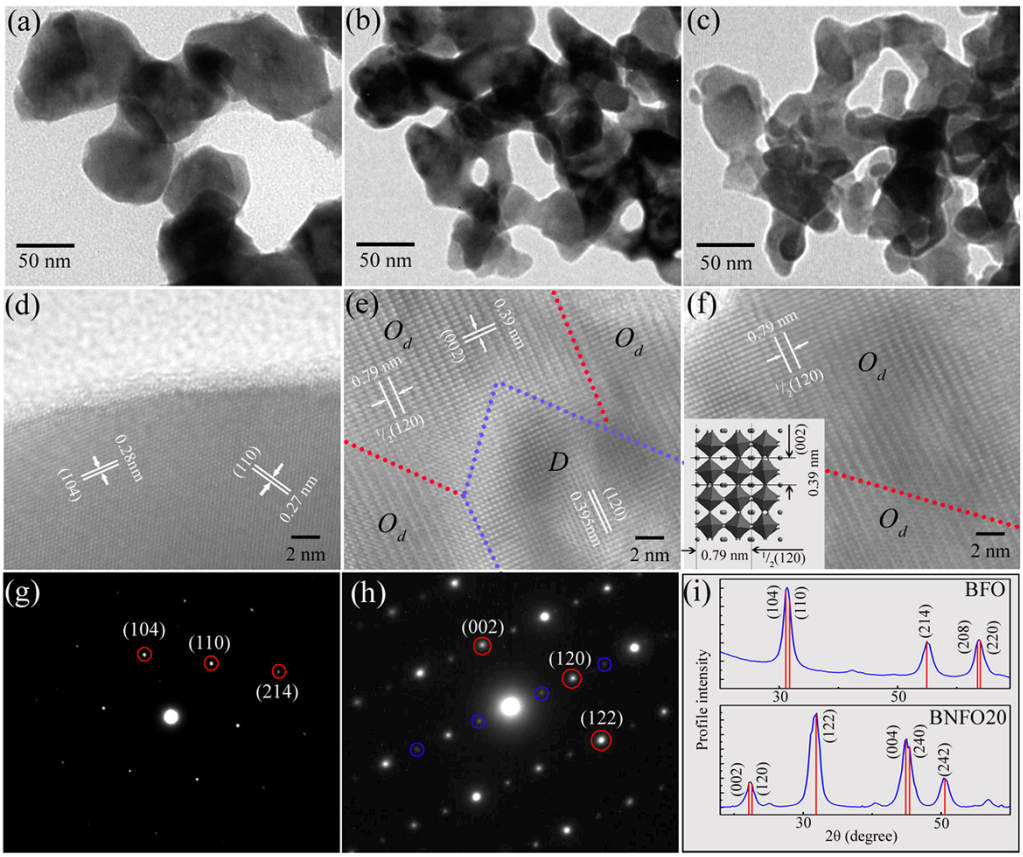

Fig. 1

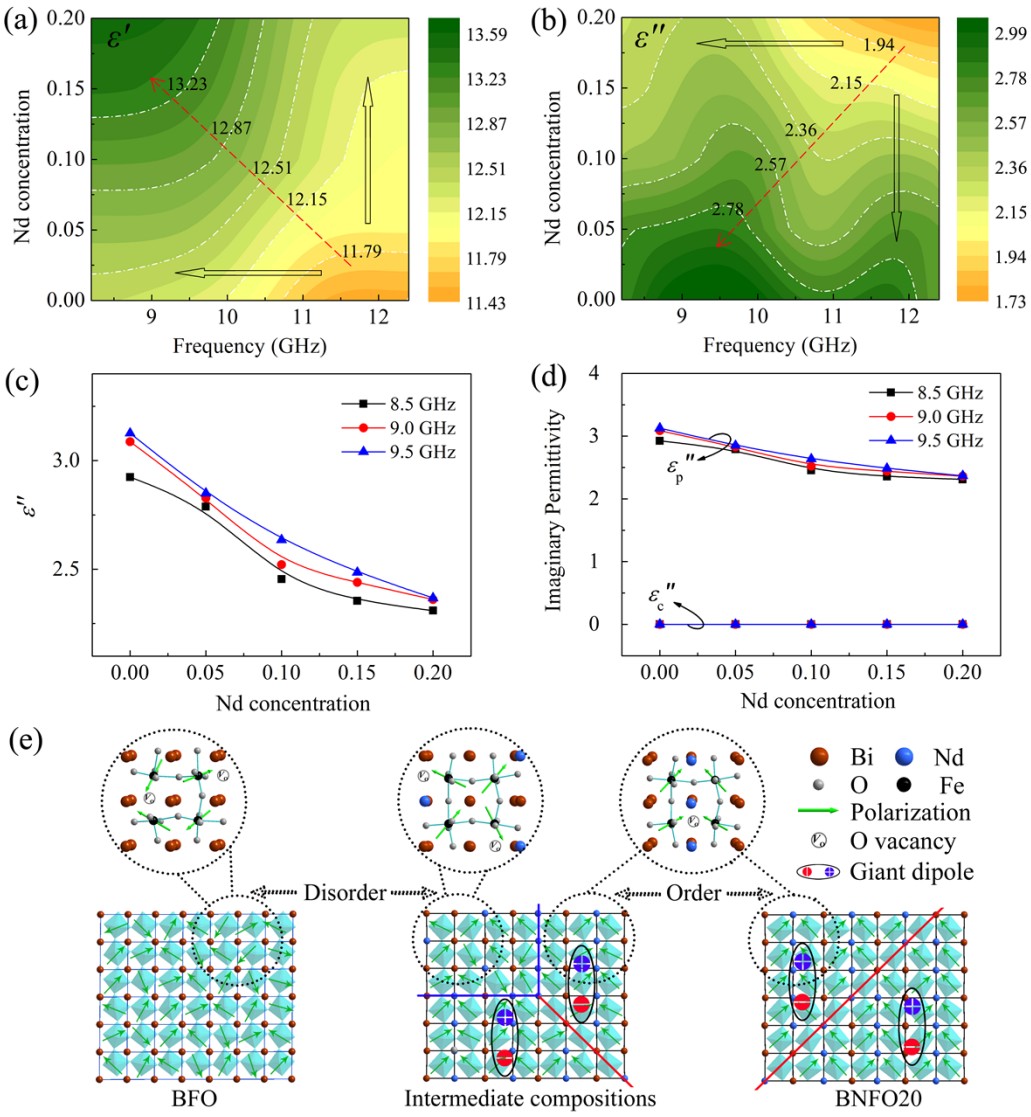

Fig. 2

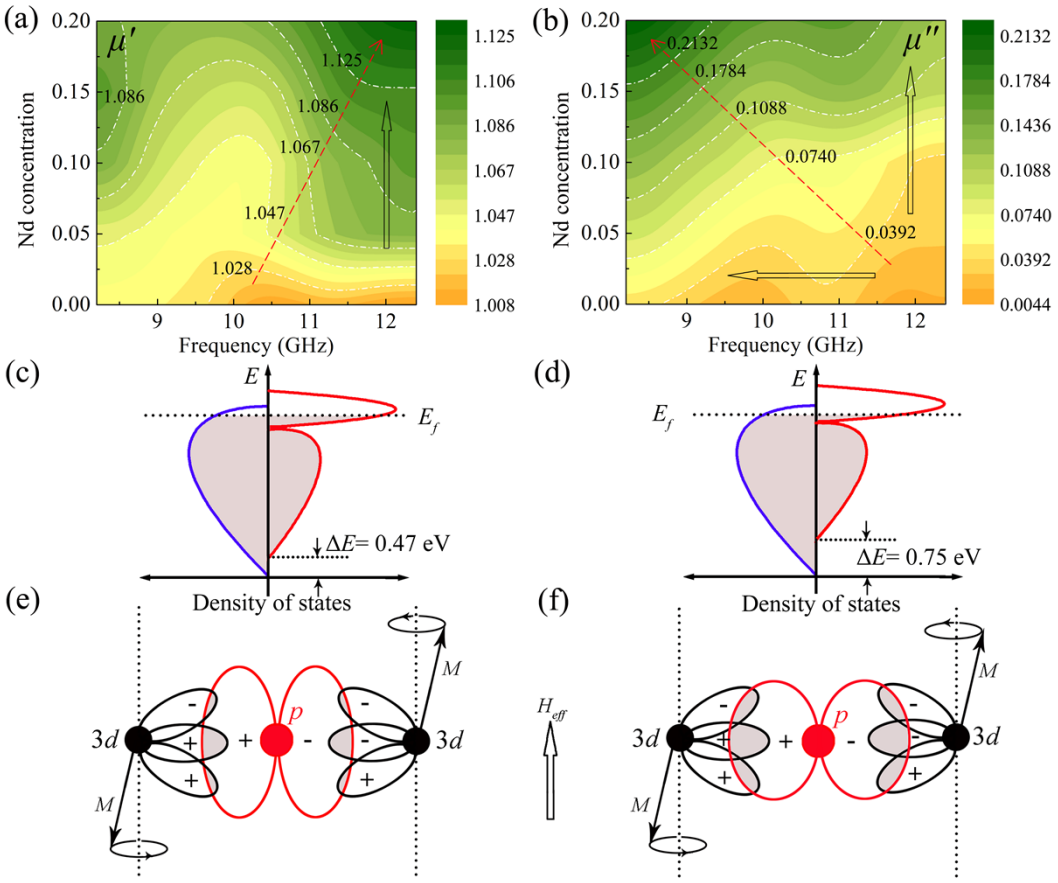

Fig. 4

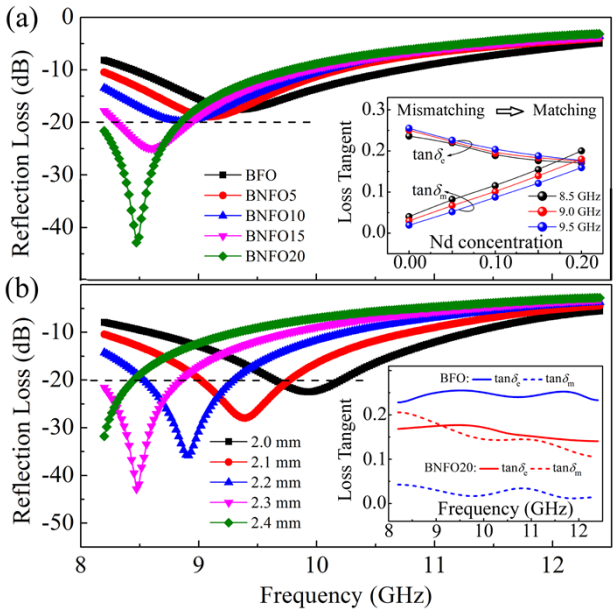

Fig. 5

A table of contents entry

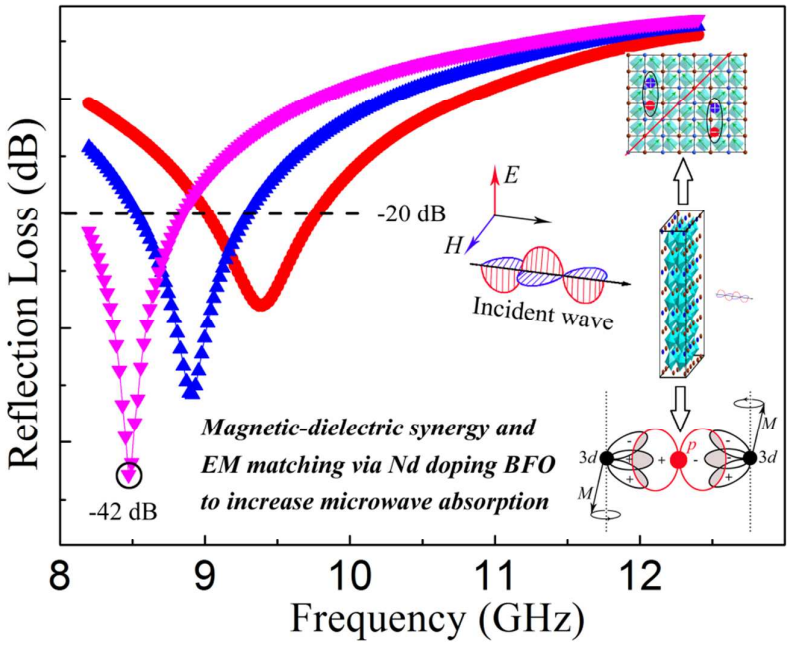

Ordering Nd doped $BiFeO_3$, novel microwave absorber, demonstrates tunable electromagnetic parameters and increased absorption due to ordering domain structure and strong superexchange interaction.